

Path and trajectory planning of a tethered UAV-UGV marsupial robotics system*

S. Martínez-Rozas¹, D. Alejo², F. Caballero³ and L. Merino²

Abstract—This paper addresses the problem of trajectory planning in a marsupial robotic system consisting of an unmanned aerial vehicle (UAV) linked to an unmanned ground vehicle (UGV) through a non-taut tether that has a controllable length. The objective is to determine a synchronized collision-free trajectory for the three marsupial system agents: UAV, UGV, and tether. First, we present a path planning solution based on optimal Rapidly exploring Random Trees (RRT*) that takes into account constraints related to the positions of UAV, UGV, tether and the 3D environment. The specialization of the main RRT* methods allows us to obtain feasible solutions in short times. Then, the paper presents a trajectory planner based on non-linear least squares. The optimizer takes into account aspects not considered in the path planning, like temporal constraints of the motion that impose limits on the velocities and accelerations of the robots. Results from simulated scenarios demonstrate that the approach is able to generate obstacle-free and smooth trajectories for the UAV, UGV, and tether.

I. INTRODUCTION

A marsupial multi-robot configuration [1] consists of a system in which one robot carries and can deploy one or several other robots of the same or different characteristics. One example is the configuration in which an Unmanned Ground Vehicle (UGV) carries an Unmanned Aerial Vehicle (UAV), which can take off and possibly land back on the UGV when needed. This configuration can be used to combine the strengths of UGVs and UAVs. This UGV-UAV marsupial configuration was used by the Team CSIRO Data61 [2], reaching second place in the DARPA 2021 Subterranean Challenge [3]. Another notable example is the Mars 2020 rover and helicopter [4]. The helicopter augments the capabilities of the rover, exploring large areas faster than the rover, providing reconnaissance on target locations and safe to traverse routes.

The flight time of small UAVs (few tens of minutes) is one of its main limiting factors. To increase their endurance, tethered UAVs fixed to a base station have been proposed [5], but the use of a tether usually limits the UAV range to a great extent. On the other hand, UGVs have a much longer autonomy, but they may not be capable of reaching certain areas of interest.

*This work has been supported by the Spanish Ministry of Science, Innovation and Universities (COMCISE RTI2018-100847-B-C22, MCIU/AEI/FEDER, UE).

¹S. Martínez-Rozas is with Universidad de Antofagasta, Antofagasta, Chile. Email: simon.martinez@uantof.cl

²D. Alejo and L. Merino are with Service Robotics Laboratory, Universidad Pablo de Olavide, Seville, Spain. Email: daletei@upo.es, fcaballero@us.es, lmercab@upo.es

³F. Caballero is with Service Robotics Laboratory, Universidad de Sevilla, Spain. Email: fcaballero@us.es

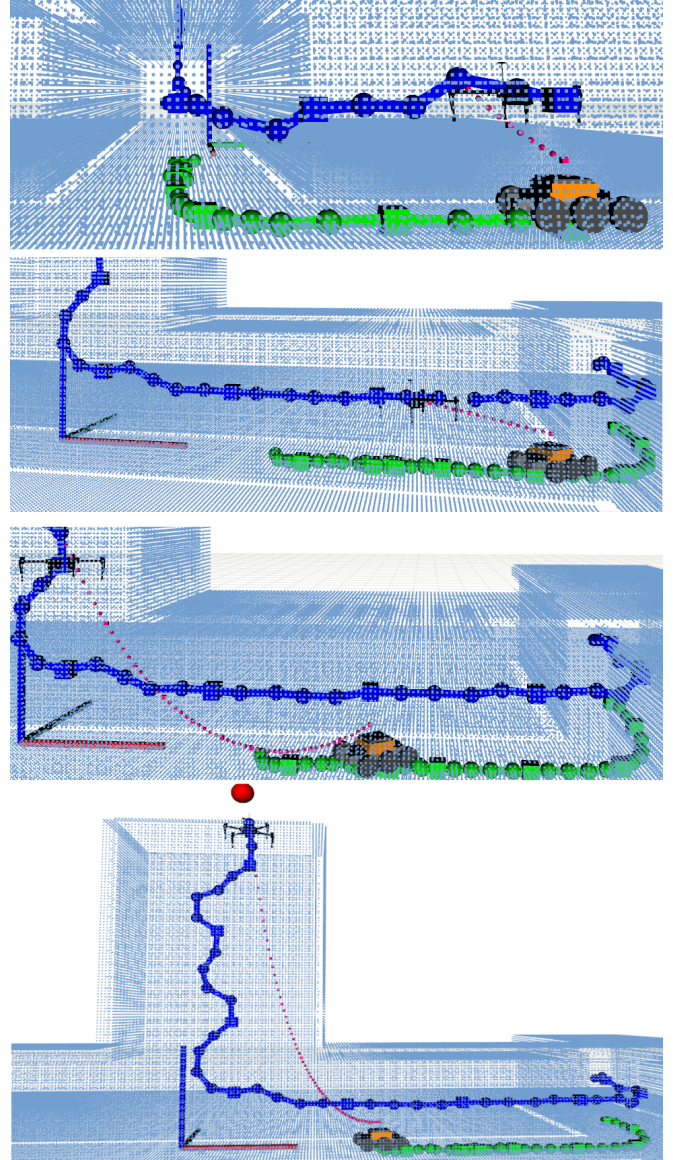


Fig. 1. Example of the developed method applied to a Marsupial robotic system. The trajectories of the UAV and UGV are represented in blue and in green, respectively. From top to bottom: first sequence after starting trajectory, with tether in red; second sequence after than UAV and UGV turning inside the tunnel, with tether in green; third sequence with UGV close to arrive to its final position and tether in red; fourth sequence with UAV close to arriving its final position, UGV set to final position and tether in red.

In this paper, we consider a tied marsupial system, composed by a UAV attached through a tether to an UGV, see Fig. 1. This configuration enables powering the UAV from

the UGV, increasing the endurance of the whole system, and, at the same time increasing flexibility over fixed tethered systems. The autonomous operation of the system requires considering the UGV-UAV-tether configuration as a whole for planning.

Thus, our goal is the development of motion planning modules for a mobile UGV-UAV-tether system. The complexity of the planning problem lies, on the one hand, in the dimension of the configuration space, in this case, the positions of UAV and UGV and the tether length. Furthermore, besides considering the collisions of each vehicle, we should also take into consideration the tether. This fact implies a large number of restrictions for the calculation of the trajectory. In our method, we do not assume a taut tether, considering the length of the tie as a control variable. This, together with the position of the UAV and UGV, allows us to be aware of the state of the tie through the mechanical model of the catenary. The contributions of the paper are:

- A path planning method for the whole system based on RRT* that determines feasible paths for UAV and UGV, and the required lengths of the tether, to achieve a desired goal configuration of the UAV.
- A trajectory planning method based on non-linear optimization that can consider smoothness, velocity and accelerations constraints of the UGV and UAV, and optimizes the tether configuration to maximize distance from obstacles.

We organized this paper as follows. Section II analyzes the existing works in the literature addressing similar problems. Then, Section III formalizes the problem to solve in this paper. The proposed method for path planning is described in Section IV. This method is used as initial solution for the non-linear optimization problem presented in Section V for trajectory planning. The experimental results are discussed in Section VI. Finally, the paper is concluded in Section VII, where we summarize the contributions of the paper and give insights of future research directions.

II. RELATED WORK

Research on tethered systems can be found for Unmanned Underwater Vehicles (UUVs) [6], as the tether is used as safety recovery device and as a communication link. However, it is usually assumed that the tethers move in a free space and thus collisions due to tethers are not considered. The use of tethers has also been applied to unmanned ground vehicles (UGVs) for exploration. In [7] a tether is used to anchor the UGV to objects in the environment in order to explore steep terrain. In [8] a UGV is tethered to a UAV, which is used as environment sensing assistance and also as an anchor to structures for climbing steep terrain. However, both approaches do not consider tethering obstacle avoidance.

In contrast, the works on motion planning for tethered UAVs and/or tethered UGV-UAV configurations are scarce. In [5], a power-tethered UAV-UGV team is presented for tasks that require longer operation and increased inspection capabilities. The authors use two independent two-

dimensional planners for each vehicle, incorporating the distinct navigation constraints and perception capabilities of each vehicle class, the power tether constraint, and relying on the RRT* algorithm for path-planning. However, the planning system operates in 2-D planes (the UGV at ground level and the UAV at a given altitude), and it does not consider the length of the tether as a control variable.

Other approaches that consider aerial robots linked with a tether usually focus on control or estimation aspects. In [9], the authors present a system in which a human is physically connected to an aerial vehicle by means of a cable. A human-state aware controller allows the robot to pull the human toward the desired position including human's velocity feedback. In [10], the use of a taut tether is proposed to increase the stability and safety in landing maneuvers. In [11], the authors consider also a tether to increase the stability when a UAV flights in confined spaces. In [12], the performance of several flight primitives for a tethered UAV is analyzed. The work describes a position and a velocity controller to follow a given trajectory for the UAV. The system controls the tether length, but assumes a taut tether to a fixed point. This is a limitation, as it forces the UAV to only access areas with direct line of sight from the fixed point.

A more complete tether state estimation is presented in [13], that describes a relative localization system for a marsupial tethered UGV-UAV pair. The estimation of the tether angles, as measured by the cable's provider SDK, and a catenary model [14] are used to estimate the relative position of the UAV with respect to the UGV. The same authors in [15] propose a PRM planner in which reachable space is constrained by the tether in two ways: avoiding any contacts of the tether with obstacles, or allowing up to two different contact points to extend the effective range. Nevertheless, again the planner assumes a tensed tether at anytime, enabling collision checking based on ray-tracing. In [16] it is presented a tethered UAV-UGV co-robots team to navigate through unstructured or confined spaces. The UAV navigates autonomously and performs as visual assistant for UGV, while UGV is tele-operated. This approach also assumes tight tether.

In [17], we proposed a trajectory planning method for an UAV tied to a fixed element. The tether length is also used as a control variable, and a loose tether and its catenary model is used to achieve configurations outside of the line of sight of the fixing point. The current work extends this one by proposing solutions to the planning problem for the UGV-UAV-tether system as a whole. This paper presents both, a path and a trajectory planner, to solve such problem. To the best of our knowledge, there are no approaches in the state of the art dealing with path or trajectory planning for a tethered UGV-UAV system considering a controllable loose tether.

III. PROBLEM STATEMENT

We define a state in the state space as the combination of the position of the UGV $\mathbf{p}_g = (x_g, y_g, z_g)^T$, the UAV $\mathbf{p}_a = (x_a, y_a, z_a)^T$ and the tether length l . At any instant,

the tether length should be longer than the distance from the UGV to the UAV, i. e. $l \geq \|\mathbf{p}_a - \mathbf{p}_g\|$. Given any state, we can obtain the shape of the tether by means of the catenary model [14], whose parameters can be computed using the Bisection Numerical Method.

The motion planning problem consists of determining the trajectory for the UGV $\mathbf{p}_g(t)$, the UAV $\mathbf{p}_a(t)$ and the tether length $l(t)$ so that the UAV reaches a given goal position, while avoiding obstacles and respecting the constraints of the system.

We discretize the trajectories, so that the states of our problem become the set:

$$O = \{\mathbf{p}_g^i, \mathbf{p}_a^i, l^i, \Delta t^i\}_{i=1, \dots, n} \quad (1)$$

where $\Delta t^i = t^i - t^{i-1}$ is the time increment between states i and $i-1$, allowing us to consider the temporal aspects. This value is the same for UGV and UAV trajectories. For each \mathbf{p}_a^i , \mathbf{p}_g^i and l^i , there is a tether configuration T^i , given by the catenary model mentioned above. When needed, we also discretize the resultant tether model into a set of m positions $\mathbf{p}_t = (x_t, y_t, z_t)$:

$$T^i = \{\mathbf{p}_t^j\}_{j=0, \dots, m-1} \quad (2)$$

IV. PATH PLANNING OF A TETHERED UAV-UGV SYSTEM USING RRT*

In our first method, we disregard the temporal aspects and, thus, the dynamic constraints of the system, tackling the path planning problem. The objective is to determine the sequence of positions for the UAV and the UGV, and the adequate tether lengths at each step, to attain the UAV goal.

Our approach makes use of the RRT* algorithm [18] to solve the problem due to its ability to deal with high-dimensional spaces. However, we do not sample in seven dimensions (UGV, UAV and tether length) to find the solution because of computational and problem domain reasons. Instead, the tether length is integrated as a constraint in the RRT* *Steering* procedure (see below), reducing the problem dimension to six. The cost function optimized in the RRT* is the weighted sum of the total length of the UAV and UGV paths, given that system states are only accepted if there exists a collision-free catenary connecting the UGV with the UAV.

In order to properly consider the constraints derived from the tethered UAV and UGV configuration, we have included specializations to the basic primitive procedures of the original RRT* algorithm [18] as we describe in detail in the following subsections.

A. RRT* problem setup

The RRT* will plan a path in a six-dimensional space composed by the UGV and UAV position $\mathbf{x} = \{\mathbf{p}_g, \mathbf{p}_a\}$, from an initial state \mathbf{x}^i to a goal UAV state \mathbf{x}^g in which only the aerial robot position is set (the final position of the UGV will depend on the UAV goal and the environment). The algorithm makes use of a 3D point cloud to represent the environment in which the robot system will plan a

path (see Fig. 2(a) as example). This point cloud is further processed for efficient obstacle representation for UAV and UGV. First, we use a method similar to [19] to perform a standard traversability analysis of the input 3D cloud to estimate the points that are traversable by the UGV, given the initial position. This traversable point cloud is used to sample UGV positions, significantly increasing the sampling efficiency (see Fig. 2(b) as example). Second, we use a more convenient representation of the UAV environment (the full 3D point cloud) using a 3D occupancy grid containing the Euclidean Distance Field (EDF) of the environment [20]. The EDF will be used to calculate the distance to obstacles from any point whenever required. Such distance can be computed with a single query to the 3D grid instead of the usual kd-tree, saving a great deal of computation effort. In our implementation, the EDF is computed off-line as part of the pipeline for the map-building process, but we can use fast EDF implementations as FIESTA [21] or VDB-EDT [22] for online computation in case of need.

B. Sampling process

When obtaining new nodes in free space through the *Sample* procedure, the UGV position \mathbf{p}_g is sampled from the points from the point cloud traversable by the UGV, and the UAV position \mathbf{p}_a from the collision free workspace. This sampling procedure allows us to plan UGV paths not only on flat surfaces but also with elevations as shown in Fig. 2(d).

C. Getting nearest node

To determine the nearest neighbor in the current tree to a new sampled configuration, the *Nearest* procedure considers a weighted sum of the Euclidean distances between the UGV and UAV positions of each node.

In terms of energy, the maneuvers of the marsupial robot system (once the UAV is flying) can be ordered from higher to lower consumption as follows: UAV hovering, UAV translation, UGV translation and stopped UGV. Thus, our approach prioritizes the UAV movement instead of the UGV (avoiding hovering) by applying a higher weight factor to the UGV component of the Euclidean distance. The nearest node is the one with the lowest cost.

D. checkCatenary algorithm

We include this algorithm during the *Steering* procedure (below) to check if there is a tether length l^i that connects the UGV and UAV steered positions without collision. The algorithm starts with the minimal possible tether length (Euclidean distance between UGV and UAV) and increases the length at fixed intervals while the tether is in collision with an obstacle at any point. When no collision is detected, and the tether does not reach the maximum length (l_{max}), the states \mathbf{p}_a^i and \mathbf{p}_g^i are considered as feasible for the length l^i , and the algorithm returns `true`.

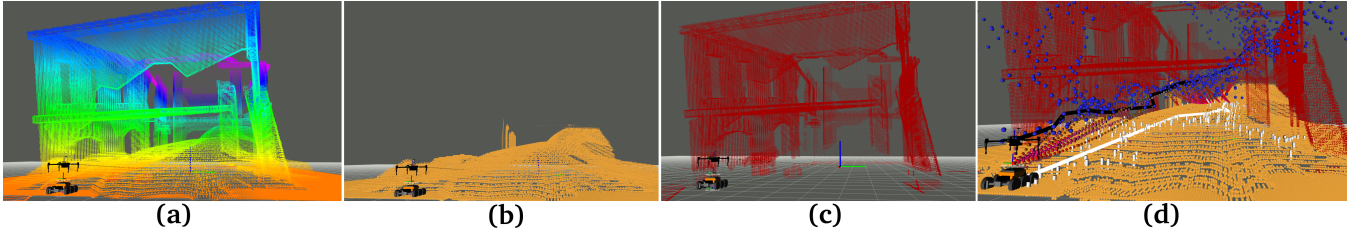


Fig. 2. (a) Example of full 3D point cloud (PC) for a scenario used for environment representation. (b) The traversable PC for the UGV computed from full cloud. (c) Obstacle PC for the UGV computed from full PC. (d) In white an example of sampling and computed path over traversable PC.

E. Steering process

The `Steering` procedure has been adapted in order to facilitate the RRT* tree growth, as well as minimizing energy consumption of the marsupial system as described in Section IV-C. According to this, three modes have been defined, from highest to lowest priority:

- 1) The first mode steers the UAV position component only, and the UGV position is fixed. If the UAV is steered without collision and `checkCatenary` is true, then the *new node* is saved.
- 2) In the case that the first mode cannot provide a viable node, the second mode is executed. The second mode steers UGV and UAV positions in such a way that if their poses are feasible and also `checkCatenary` is true, the *new node* is saved. Otherwise, the third mode is executed.
- 3) The last mode just steers the UGV and considers the UAV fixed. Then, if the UGV pose is feasible and `checkCatenary` is true, the *new node* is saved.

Finally, if a *new node* was not found in any one of three modes, a new *random node* is calculated using `Sample`.

F. Collision test

In the `CollisionFree` process, not only is the new node checked, but also the feasibility to move from the *nearest node* to the *new node* is checked. For that we interpolate the whole state between those nodes, and check for collisions and the existence of catenary in each one of the interpolated states.

V. TRAJECTORY PLANNING OF A TETHERED UAV-UGV SYSTEM USING NON-LINEAR OPTIMIZATION

The result of the path planning method from the previous section is a sequence of feasible states $\{\mathbf{p}_g^i, \mathbf{p}_a^i, l^i\}_{i=1, \dots, n}$ that avoids collisions. This sequence is a partial solution to (1), which does not consider kinematic and dynamic constraints. Furthermore, the tether lengths, while adequate to avoid obstacles, are not optimized for safety (distance to obstacles).

In this section, we present a trajectory planning approach based on non-linear optimization that provides the final solution to (1). The planner uses the result of the previous section as the initial solution, as described next.

A. Initial trajectory estimation

The first step consists on adding time information to the initial path as the initial trajectory solution. For that, we take into account two main aspects.

The first one aims to adjust the initial sequence to have a set of equi-distant waypoints. RRT* creates nodes at a given distance (epsilon) from their parents, which is convenient for us as we aim to sample the trajectory at regular intervals. However, because our proposed `Steering` process (Section IV-E), we can get packed way-points at the same position in the case of the UGV. To avoid this, whenever we detect some grouped points we spread them evenly to reach the next non-grouped point. Note that as we check for feasibility in the nodes connecting consecutive states (see Section IV-F), the new points are feasible. Furthermore, for each point, the tether length is calculated through the `checkCatenary` procedure.

Then, the Δt^i values are initialized. To do so, scalar constant speeds, v_g and v_a , are imposed over UGV and UAV path respectively. For consistency, both trajectories must use the same Δt^i to coordinate that UGV and UAV reach the way-point at the same time.

Thus, Δt^i value for each state of (1) is computed considering the largest value between $\|\mathbf{p}_g^i - \mathbf{p}_g^{i+1}\|/v_g$ and $\|\mathbf{p}_a^i - \mathbf{p}_a^{i+1}\|/v_a$.

B. Casting the problem as a sparse non-linear optimization

Based on the discretization of the states (1), our problem consists of determining the values of the variables in O that optimize a weighted multi-objective function $f(O)$:

$$O^* = \arg \min_O f(O) = \arg \min_O \sum_{i,k} \gamma_k * \|\delta_k^i(O)\|^2 \quad (3)$$

O^* denotes the optimized collision-free trajectory for UAV, UGV and tether from the starting and goal configurations. γ_k is the weight for each component $\delta_k(O)$ (also known as residual) of the objective function. Each component encodes a different constraint or optimization objective of our problem, and will be presented next. Besides, each component should be evaluated in all the timesteps i of the trajectory. These components are local with respect to i , as they only depend on a few number of consecutive states in general. Consequently, our optimization problem can be solved with non-linear sparse optimization algorithms. In particular, we use *Ceres-Solver* [23] as our optimization back-end.

C. Constraints and Objective Function

We represent the constraints in the problem as penalty costs in the objective function. The proposed constraints are related to the tether length, the limits on velocity and acceleration, and the equi-distance among consecutive robot poses. In addition, we aim to maximize the distance from obstacles to each marsupial system agent, minimize the execution time of the trajectory, and maximize the trajectory smoothness.

1) *Equi-distance among states trajectory*: The optimization process might move UGV and/or UAV positions within the planning space in order to minimize the costs of the different constraints. In the optimization process, the positions of the UGV and UAV are likely to be grouped in low-cost areas. To avoid it, we force them to keep a given distance among states, ρ_{eg} for the UGV and ρ_{ea} for the UAV. This distance is the path distance between the initial and goal points divided by the number of the steps in the trajectory.

$$\delta_{eg}^i = \|p_g^{i+1} - p_g^i\| - \rho_{eg} \quad (4)$$

$$\delta_{ea}^i = \|p_a^{i+1} - p_a^i\| - \rho_{ea} \quad (5)$$

2) *UAV Obstacle avoidance*: This constraint penalizes the UAV states whose distance to nearest obstacle d_{oa}^i is closer than a safety distance ρ_{oa} . Where ρ_{oa} is a parameter which depends on the dimension of the UAV.

$$\delta_{oa}^i = \begin{cases} \rho_{oa} - d_{oa}^i & , \text{if } d_{oa}^i < \rho_{oa} \\ 0 & , \text{otherwise} \end{cases} \quad (6)$$

3) *Tether Obstacle avoidance*: The tether state is computed by solving the catenary model for l^i between \mathbf{p}_g^i and \mathbf{p}_a^i . The catenary is sampled according to (2) into m points. This constraint penalizes the proximity of the sampled tether to obstacles. We compute the distance to the nearest obstacles of every sample of tether l_i , $d_{ot,j}^i$, and estimate the residual as the sum of the inverse nearest distances. We increase the weight of those samples closer than a safety distance ρ_{ot} to guarantee higher cost in these cases using $\rho_j = \beta$, with $\beta \gg 1$.

$$\delta_{ot}^i = \sum_{j=0}^{m-1} \frac{\rho_j}{d_{ot,j}^i}, \quad \rho_j = \begin{cases} 1 & , \text{if } d_{ot,j}^i > \rho_{ot} \\ \beta & , \text{otherwise} \end{cases} \quad (7)$$

4) *UGV Obstacle avoidance*: This constraint penalizes the UGV states whose distance to the nearest obstacle d_{og}^i is closer than a safety distance ρ_{og} . Where ρ_{og} is a parameter which depends on the dimension of the UGV.

$$\delta_{og}^i = \begin{cases} \rho_{og} - d_{og}^i & , \text{if } d_{og}^i < \rho_{og} \\ 0 & , \text{otherwise} \end{cases} \quad (8)$$

5) *UGV Traversability*: It is necessary for the UGV to remain in traversable areas. To this end, we impose a δ_{trav} penalty to the UGV states that are away a distance d_{trav}^i

from traversable surface larger than ρ_{trav} . Thus, d_{trav}^i is the distance to the closest point into the traversable point cloud.

$$\delta_{trav}^i = \begin{cases} d_{trav}^i - \rho_{trav} & , \text{if } d_{trav}^i > \rho_{trav} \\ 0 & , \text{otherwise} \end{cases} \quad (9)$$

6) *Smoothness*: This constraint is in charge of avoiding abrupt direction changes for UGV and UAV trajectories. From three consecutive positions, two vectors are calculated. The first between i and $i-1$ states, and the second between $i+1$ and i states. Then, we calculate the angle between these vectors, θ_g for the UGV, and θ_a for the UAV. The residuals δ_{sg} and δ_{sa} penalize the states whenever the angle between vectors exceeds a given threshold ρ_{sg} and ρ_{sa} respectively:

$$\cos(\theta_g) = \frac{(\mathbf{p}_g^i - \mathbf{p}_g^{i-1})^T (\mathbf{p}_g^{i+1} - \mathbf{p}_g^i)}{\|\mathbf{p}_g^i\| \|\mathbf{p}_g^{i+1}\|} \quad (10)$$

$$\cos(\theta_a) = \frac{(\mathbf{p}_a^i - \mathbf{p}_a^{i-1})^T (\mathbf{p}_a^{i+1} - \mathbf{p}_a^i)}{\|\mathbf{p}_a^i\| \|\mathbf{p}_a^{i+1}\|} \quad (11)$$

$$\delta_{sg}^i = \begin{cases} \cos(\theta_g) - 1, & \text{if } |\theta_g| > \rho_{sg} \\ 0, & \text{otherwise} \end{cases} \quad (12)$$

$$\delta_{sa}^i = \begin{cases} \cos(\theta_a) - 1, & \text{if } |\theta_a| > \rho_{sa} \\ 0, & \text{otherwise} \end{cases} \quad (13)$$

7) *Trajectory duration time*: This constraint is in charge of minimizing the difference between the trajectory time between two consecutive states and the ones from the initial solution.

$$\delta_t^i = \Delta t^i - \Delta t_{[0]}^i \quad (14)$$

where $\Delta t_{[0]}^i$ and Δt^i are the time difference between the steps $i-1$ and i in the initial solution and in the current trajectory respectively.

8) *Velocity*: This constraint relates two consecutive positions states and the time step between them, for the UGV and the UAV. It is in charge of keeping the speed for both the UGV and the UAV during the optimized trajectory as constant as possible. Then, the error δ_v corresponds to the difference between the computed states velocity and the desired velocity ρ_v .

$$\delta_{vg}^i = v_g^i - \rho_{vg} \quad (15)$$

$$\delta_{va}^i = v_a^i - \rho_{va} \quad (16)$$

where $v_g^i = \frac{|\mathbf{p}_g^{i+1} - \mathbf{p}_g^i|}{\Delta t^{i+1}}$ and $v_a^i = \frac{|\mathbf{p}_a^{i+1} - \mathbf{p}_a^i|}{\Delta t^{i+1}}$ are the velocity between two consecutive poses for the UGV and the UAV, respectively.

9) *Acceleration*: It relates three consecutive positions and their related time steps for the UGV and the UAV. The idea is to keep the linear acceleration close to zero in order to minimize the control efforts.

$$\delta_{ag}^i = \frac{v_g^i - v_g^{i-1}}{\Delta t^i + \Delta t^{i+1}} \quad (17)$$

$$\delta_{aa}^i = \frac{v_a^i - v_a^{i-1}}{\Delta t^i + \Delta t^{i+1}} \quad (18)$$

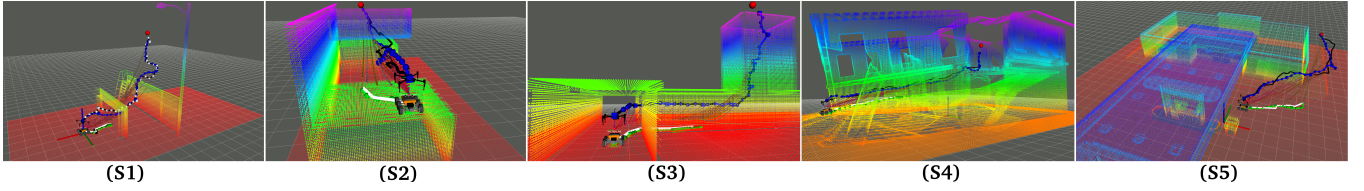


Fig. 3. Scenarios considered for validation. S1: Open/constrained space with arc as obstacle. S2: Narrow/constrained space with denied access to UGV. S3: Confined space with outlet duct for UAV. S4: Collapsed Fire Station. S5: Open space gas station.

10) *Unfeasible tether length*: This constraint penalizes unfeasible tether lengths, that is, tethers with length l^i shorter than the Euclidean distance between \mathbf{p}_g^i and \mathbf{p}_a^i , d_u^i . We heavily penalize unfeasible tethers by means of an exponential error.

$$\delta_u^i = \begin{cases} (e^{d_u^i - l^i}) - 1 & , \text{if } d_u^i > l^i \\ 0 & , \text{otherwise} \end{cases} \quad (19)$$

VI. EXPERIMENTAL RESULTS

Both methods, path and trajectory planners, have been implemented in C++, and the full approach as a planner in Robot Operating System (ROS). The source code is publicly available¹. The *Ceres-Solver* [23] has been selected as the back-end to model and solve the optimization problem.

To validate the feasibility of the proposed approach, we have conceived a set of experiments in five simulated environments, with different degrees of complexity (see Fig. 3). For better understanding, we have included an accompanying video² that summarizes each of the experiments in the different scenarios. The scenario features are: open/constrained space (scenario S1), narrow/constrained space (scenario S2), confined spaces (scenarios S3 and S4) and open spaces (scenario S5). Our methods are able to find solutions in environments and tasks where approaches that assume a taut tether and/or a fixed UGV pose would fail. As an example, let us consider the performance of our method in S3, see Fig 1, where the UAV must turn inside a corridor and then move inside a chimney to reach the goal. For that, the UGV should enter into the corridor, moving close to chimney to enable the UAV entering into it.

For each scenario, we compute a path for the whole system using the RRT* method. Then, this method is used as the initial solution to obtain the trajectory using the non-linear optimization approach. The RRT* is set to have a maximum of 50000 iterations. If one or more solutions are found in intervals of 500 iterations, then the RRT* algorithm stops and the current solution is used as initial path in the optimization process. To define such iteration limit we performed experiments in scenarios with different complexity, in most cases a good solution was found after 1000 iterations.

All the experiments have been executed 100 times and with the same set of parameters. We also tested the methods in two different initial position for each scenario. The

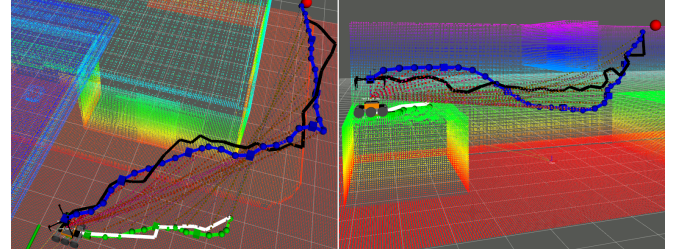


Fig. 4. Trajectories in S5 and S2. The lines blue and green are the optimized trajectories for UAV and UGV respectively, and, the lines black and white are initial path UAV and UGV respectively.

maximum number of optimizer iterations are one thousand. The parameters used for the experimental results are detailed below, the weight factors are all normalized from 0 to 1:

- Weighting factors for UGV: $\gamma_{eg} = 0.2$, $\gamma_{og} = 0.08$, $\gamma_{trav} = 0.5$, $\gamma_{sg} = 0.12$, $\gamma_{vg} = 0.05$, $\gamma_{ag} = 0.005$.
- Weighting factors for UAV: $\gamma_{ea} = 0.25$, $\gamma_{oa} = 0.08$, $\gamma_{sa} = 0.14$, $\gamma_{va} = 0.05$, $\gamma_{aa} = 0.005$.
- Weighting factors for Tether: $\gamma_{ot} = 0.25$, $\gamma_u = 0.1$
- Weighting factor Time: $\gamma_t = 0.001$.
- Equi-distance threshold: ρ_{eg} and ρ_{ea} are computed based on the initial path.
- Collision threshold: $\rho_{oa} = 1.2$, $\rho_{ot} = 0.1$, $\rho_{og} = 1.2$.
- Traversability threshold: $\rho_{trav} = 0.001$.
- Smoothness threshold: $\rho_{sg} = \frac{\pi}{9}$, $\rho_{sa} = \frac{\pi}{9}$.
- Velocity threshold: $\rho_{vg} = 1.0$, $\rho_{va} = 1.0$.
- Tether avoidance: $\beta = 10.0$.

The results of the experiments are summarized and detailed in Tables I and II. The presented metrics are the following:

- SI: Scenario - Initial Position
- F: Feasibility
- TCI: Compute Time for initial solution
- TCO: Compute Time for optimized solution
- VTI: Velocity of the initial trajectory [m/s]
- VTO: Velocity of the optimized trajectory [m/s]
- ATI: Acceleration of the initial trajectory [m/s²]
- ATO: Acceleration of the optimized trajectory [m/s²]
- LIP: Length of initial path [m]
- LTO: Length of the optimized trajectory [m]
- DOI: Distance obstacles-initial path [m]
- DOO: Distance obstacles-optimized trajectory [m]
- DCOI: Dist. catenary-obstacle solution initial [m]
- DCOO: Dist. catenary-obstacles solution optimized[m]

In order to benchmark the solution, we use as baseline the value of the different metrics prior to optimization, that

¹https://github.com/robotics-upo/marsupial_optimizer, branch: noetic

²<https://youtu.be/mewpnyUU7Y>

is, the solution of the RRT* detailed in Section IV. Next paragraphs evaluate the different metrics.

A. Feasibility

The result of the planners is considered as feasible when the computed path/trajectory is collision free for every agent of the system. This means that $d_{og}^i > \rho_{og}$ and $d_{oa}^i > \rho_{oa}$ for every UGV and UAV state respectively. In case of tether, $d_{ot,j}^i > \rho_{ot}$ for every tether sample in each tether configuration.

A first important result is that the RRT* planner is able to find a feasible solution in 100% of the cases, despite the number of dimensions of the problem, in a short time in most of the cases. On the other hand, the feasibility of the trajectory planner is 86.6%. In 99% of the unfeasible solutions, the reason is a collision of the tether with an obstacle. The optimizer considers more constraints than the RRT*, as dynamics, distance to obstacles, equidistant, etc. These new constraints might sometimes move the solution relatively far from the initial guess provided by the RRT*. Additionally, the tether obstacle avoidance constraint (7) can only be computed numerically by the solver, making its gradient more sensible to numerical issues. As a result, the optimizer might produce unfeasible solutions when checking complex configurations far from the initial solution.

B. Trajectory length and elapsed time

The trajectory planner does not minimize trajectory length explicitly. The constraints influence the length of the optimized trajectories, increasing their value compared to the initial one. This is either by moving away from obstacles, by increasing the curvature of the trajectory to smooth it, or even to get a equi-distance between states. As consequence the trajectory is safer, smoother, and easier to maneuver, see Fig. 4.

C. Distance to obstacles

The distance to obstacle statistics shown in Table II (DOI, DOO, DCOI, DCOO) for UGV and UAV confirm how the optimized trajectory tends to move away from obstacles when the trajectory itself is closer than the safety distance. For the tether, the DCOO min is on average above the considered safety value ρ_{ot} . The DCOI and DCOO mean values are similar for both methods.

D. Velocities and Accelerations

The results in Table I show how the velocity and acceleration after optimization (VTO, ATO) are close to the desired values, which are 1.0 m/s and 0 m/s^2 respectively. There is a noticeable improvement on these values w.r.t the initial ones.

E. Smoothness

Figure 4 represents the final trajectory as obtained by our trajectory planning method in blue and green lines for UAV and UGV respectively. It can be compared to the initial path, represented in black and white lines for UAV and UGV, respectively. By introducing the smoothness cost, we can improve the smoothness of the initial path given by RRT*.

F. Computational Time

Table I presents a summary of the computation time (TCI, TCO) required to estimate both the initial and optimized trajectories. We used a 9th gen Intel Core i7 running at 2.20GHz with 32 GB of RAM. The results indicate that the RRT* algorithm is able to obtain a solution faster in confined and narrow/constrained scenarios (around 0.5 seconds). In contrast, it can raise to 27.9 seconds in open spaces. On the other hand, the optimization algorithm requires significantly longer times to reach the solution due to the complexity of solving within the optimizer the transcendental equations of the catenary model. Several strategies, such as using tri-linear approximations of the Distance Function to analytically approximate its gradient (as we do in [24]) or approximating the shape of the catenary could be considered to reduce the computation time of the optimization stage. We will consider such improvements as future work.

VII. CONCLUSIONS AND FUTURE WORK

This paper presented a general path and trajectory planning algorithm for a marsupial system. Contrary to most approaches in the state of the art, our methods do not assume a taut tether, using the catenary model instead. This model generalizes the tether parametrization, considering both taut and loose configurations.

The planning methods have been tested in challenging simulation environments in which the solution need of UGV translation and a loose tether to properly reach the goal position.

Despite the size of the problem to be solved, using the adapted RRT* algorithm provides solutions in few seconds, and with a feasibility of 100%.

The optimization process generates safer trajectories than planner in terms of distance to obstacles, especially related to UGV and UAV agents. Unfortunately, the trajectory planner requires significant computation effort, preventing its online use.

Future work will consider validating the method in experiments involving real robots. We are also developing analytical approximations to speed up the computation of the parameters and the state of the catenary model. Analytical approximations of the catenary model will also improve error gradient estimation, with the corresponding impact on both accuracy and feasibility.

REFERENCES

- [1] R. Murphy, M. Ausmus, M. Bugajska, T. Ellis, T. Johnson, N. Kelley, J. Kiefer, and L. Pollock, "Marsupial-like mobile robot societies," in *AGENTS '99*, 1999.
- [2] N. Hudson, F. Talbot, M. Cox, J. Williams, T. Hines, A. Pitt, B. Wood, D. Frousheger, K. L. Surdo, T. Molnar, R. Steindl, M. Wildie, I. Sa, N. Kottege, K. Stepanas, E. Hernandez, G. Catt, W. Docherty, B. Tidd, B. Tam, S. Murrell, M. Bessell, L. Hanson, L. Tychsen-Smith, H. Suzuki, L. Overs, F. Kendoul, G. Wagner, D. Palmer, P. Milani, M. O'Brien, S. Jiang, S. Chen, and R. C. Arkin, "Heterogeneous Ground and Air Platforms, Homogeneous Sensing: Team CSIRO Data61's Approach to the DARPA Subterranean Challenge," 2021.
- [3] DARPA, "DARPA SUBTERRANEAN CHALLENGE 2021," <https://www.subtchallenge.com/index.html>, 2021.

TABLE I
RESULTS FOR FEASIBILITY, COMPUTE TIME AND TRAJECTORY TIME PARAMETERS IN SIMULATED ENVIRONMENTS

ALL				UGV								UAV							
SI	F	TCI	TCO	Mean VTI	Max VTI	Mean VTO	Max VTO	Mean ATI	Max ATI	Mean ATO	Max ATO	Mean VTI	Max VTI	Mean VTO	Max VTO	Mean ATI	Max ATI	Mean ATO	Max ATO
S1.1	86.0	5.1	465.9	0.37	0.78	0.36	1.07	-0.23	0.15	0.02	0.81	0.88	1	0.97	1.19	-0.74	0.25	-0.002	-0.09
S1.2	70.0	15.0	529.7	0.50	0.97	0.43	1.25	-0.26	0.22	0.02	0.78	0.87	1	0.91	1.19	-0.72	0.32	-0.002	-0.08
S2.1	94.5	0.4	123.6	0.11	0.31	0.13	0.91	-0.11	0.16	0.02	0.96	0.92	1	1.01	1.15	-0.71	0.06	0.002	0.01
S2.2	95.0	0.5	109.3	0.27	0.70	0.19	1.00	-0.15	0.15	0.03	1.09	0.92	1	0.99	1.09	-0.70	0.11	0.000	0.07
S3.1	84.8	0.5	213.6	0.43	0.90	0.50	1.07	-0.29	0.30	0.00	0.21	0.88	1	1.02	1.21	-0.73	0.20	0.003	0.16
S3.2	84.0	1.5	214.9	0.49	0.96	0.55	1.08	-0.31	0.34	0.00	-0.20	0.85	1	0.98	1.16	-0.69	0.26	0.004	0.18
S4.1	82.5	1.2	539.0	0.57	0.98	0.45	1.14	-0.33	0.24	0.02	1.00	0.88	1	0.94	1.12	-0.71	0.30	-0.002	-0.06
S4.2	76.0	12.8	708.6	0.43	0.96	0.47	1.32	-0.25	0.23	0.01	0.86	0.87	1	0.92	1.22	-0.70	0.40	-0.002	-0.32
S5.1	98.0	27.9	277.8	0.45	0.95	0.41	1.15	-0.23	0.25	0.03	1.07	0.87	1	0.97	1.27	-0.64	0.25	-0.004	-0.14
S5.2	95.0	26.0	447.7	0.67	1.00	0.57	1.08	-0.41	0.43	0.02	1.02	0.88	1	0.92	1.11	-0.68	0.39	-0.004	-0.12

TABLE II
RESULTS FOR TIME, TRAJECTORY LENGTH AND OBSTACLE DISTANCE IN SIMULATED ENVIRONMENTS

ALL	UGV						UAV						Tether			
SI	LIP	LTO	Mean DOI	Min DOI	Mean DOO	Min DOO	LIP	LTO	Mean DOI	Min DOI	Mean DOO	Min DOO	Mean DCOI	Min DCOI	Mean DCOO	Min DCOO
S1.1	6.3	6.3	2.26	1.45	2.28	1.55	14.6	14.2	1.83	0.65	1.87	0.80	1.15	0.31	1.14	0.25
S1.2	10.7	10.8	3.74	1.50	3.76	1.60	18.8	18.2	2.20	0.85	2.21	0.89	1.30	0.22	1.31	0.16
S2.1	1.5	1.6	0.65	0.56	0.69	0.56	13.1	12.7	1.10	0.59	1.19	0.76	0.71	0.13	0.72	0.10
S2.2	2.7	2.7	0.75	0.58	0.75	0.58	13.4	13.1	1.11	0.56	1.16	0.67	0.75	0.17	0.75	0.13
S3.1	8.6	8.9	0.88	0.50	0.98	0.62	17.7	17.6	0.69	0.51	0.81	0.56	0.68	0.20	0.67	0.13
S3.2	11.1	11.4	0.88	0.50	0.97	0.61	19.0	18.9	0.69	0.50	0.79	0.54	0.68	0.23	0.67	0.14
S4.1	10.8	10.8	2.12	1.39	2.12	1.40	20.9	20.7	1.09	0.53	1.16	0.65	0.80	0.22	0.74	0.14
S4.2	15.4	16.0	1.70	1.02	1.70	1.07	27.1	26.7	1.06	0.51	1.15	0.65	0.82	0.22	0.76	0.10
S5.1	9.4	9.2	2.24	0.70	2.26	0.76	18.5	18.1	1.71	0.72	1.74	0.83	1.12	0.30	1.09	0.23
S5.2	23.7	23.3	2.52	0.59	2.53	0.63	35.2	34.9	1.65	0.58	1.66	0.65	1.17	0.25	1.14	0.22

- [4] H. F. Grip, D. P. Scharf, C. A. Malpica, W. Johnson, M. Mandic, G. Singh, and L. A. Young, "Guidance and control for a mars helicopter," in NASA, 2018.
- [5] C. Papachristos and A. Tzes, "The power-tethered uav-ugv team: A collaborative strategy for navigation in partially-mapped environments," in *22nd Mediterranean Conference on Control and Automation*, 2014, pp. 1153–1158.
- [6] M. Laranjeira, C. Dune, and V. Hugel, "Catenary-based visual servoing for tether shape control between underwater vehicles," *Ocean Engineering*, vol. 200, p. 107018, 2020.
- [7] T. Miki, P. Khrapchenkov, and K. Hori, "Uav/ugv autonomous cooperation: Uav assists ugv to climb a cliff by attaching a tether," in *2019 International Conference on Robotics and Automation (ICRA)*, 2019, pp. 8041–8047.
- [8] P. McGarey, F. Pomerleau, and T. D. Barfoot, *System Design of a Tethered Robotic Explorer (TRex) for 3D Mapping of Steep Terrain and Harsh Environments*. Cham: Springer International Publishing, 2016, pp. 267–281. [Online]. Available: https://doi.org/10.1007/978-3-319-27702-8_18
- [9] M. Allenspach, Y. Vyas, M. Rubio, R. Siegwart, and M. Tognon, "Human-state-aware controller for a tethered aerial robot guiding a human by physical interaction," *IEEE Robotics and Automation Letters*, pp. 1–1, 2022.
- [10] L. A. Sandino, D. Santamaria, M. Bejar, A. Viguria, K. Kondak, and A. Ollero, "Tether-guided landing of unmanned helicopters without gps sensors," in *2014 IEEE International Conference on Robotics and Automation (ICRA)*, 2014, pp. 3096–3101.
- [11] M. Schulz, F. Augugliaro, R. Ritz, and R. D'Andrea, "High-speed, steady flight with a quadcopter in a confined environment using a tether," in *2015 IEEE/RSJ International Conference on Intelligent Robots and Systems (IROS)*, 2015, pp. 1279–1284.
- [12] X. Xiao, J. Dufek, and R. Murphy, "Benchmarking tether-based uav motion primitives," in *2019 IEEE International Symposium on Safety, Security, and Rescue Robotics (SSRR)*, 2019, pp. 51–55.
- [13] J. D. X. Xiao, Y. Fan and R. Murphy, "Indoor uav localization using a tether," in *2018 IEEE International Symposium on Safety, Security, and Rescue Robotics (SSRR)*, Philadelphia, PA, 2018. IEEE, 2018, pp. 1–6.
- [14] E. Lockwood, *A Book of Curves*, 1st ed. Cambridge University Press, ISBN: 103156, 1961.
- [15] X. Xiao, J. Dufek, M. Suhail, and R. Murphy, "Motion planning for a uav with a straight or kinked tether," in *2018 IEEE/RSJ International Conference on Intelligent Robots and Systems (IROS)*, Madrid, 2018. IEEE, 2018, pp. 8486–8492.
- [16] X. Xiao, J. Dufek, and R. Murphy, "Autonomous visual assistance for robot operations using a tethered uav," in *Field and Service Robotics*, 01 2021, pp. 15–29.
- [17] S. Martinez-Rozas, D. Alejo, F. Caballero, and L. Merino, "Optimization-based trajectory planning for tethered aerial robots," *ICRA 2021*, 2021.
- [18] S. Karaman and E. Frazzoli, "Sampling-based algorithms for optimal motion planning," *The International Journal of Robotics Research*, vol. 30, no. 7, pp. 846–894, 2011.
- [19] P. Krüsi, P. Furgale, M. Bosse, and R. Siegwart, "Driving on point clouds: Motion planning, trajectory optimization, and terrain assessment in generic nonplanar environments," *Journal of Field Robotics*, vol. 34, no. 5, pp. 940–984, 2017. [Online]. Available: <https://onlinelibrary.wiley.com/doi/abs/10.1002/rob.21700>
- [20] H. Oleynikova, A. Millane, Z. Taylor, E. Galceran, J. I. Nieto, and R. Y. Siegwart, "Signed distance fields: A natural representation for both mapping and planning," 2016.
- [21] L. Han, F. Gao, B. Zhou, and S. Shen, "FIESTA: fast incremental euclidean distance fields for online motion planning of aerial robots," in *2019 IEEE/RSJ International Conference on Intelligent Robots and Systems, IROS 2019, Macau, SAR, China, November 3-8, 2019*. IEEE, 2019, pp. 4423–4430.
- [22] D. Zhu, C. Wang, W. Wang, R. Garg, S. A. Scherer, and M. Q. Meng, "VDB-EDT: an efficient euclidean distance transform algorithm based on VDB data structure," *Under Review*, vol. abs/2105.04419, 2021. [Online]. Available: <https://arxiv.org/abs/2105.04419>
- [23] S. Agarwal, K. Mierle, and Others, "Ceres solver," <http://ceres-solver.org>, 2021.
- [24] F. Caballero and L. Merino, "DLL: Direct LIDAR Localization. A map-based localization approach for aerial robots," in *2021 IEEE/RSJ International Conference on Intelligent Robots and Systems (IROS)*, 2021, pp. 5491–5498.